Mutational profiling of micro-dissected pre-malignant lesions from archived specimens

Daniela Nachmanson[1], Joseph Steward[2], Huazhen Yao[3], Eliza Jeong[2], Thomas J. O'Keefe[4], Farnaz Hasteh[5], Kristen Jepsen[3], Gillian L. Hirst[7], Laura J. Esserman[7], Alexander D. Borowsky[8], Olivier Harismendy[2,6,†]

1. Bioinformatics and Systems Biology Graduate Program - UC San Diego, 9500 Gilman Dr., La Jolla, CA 92093, 2. Moores Cancer Center - 3855 Health Sciences Dr., La Jolla, CA 92093, 3. Institute for Genomic Medicine - UC San Diego, 9500 Gilman Dr., La Jolla, CA 92093, 4. Division of Breast Surgery And The Comprehensive Breast Health Center – UC San Diego 3855 Health Sciences Dr., La Jolla, CA 92093. 5. Department of Pathology - UC San Diego 9500 Gilman Dr., La Jolla, CA 92093, 6. Division of Biomedical Informatics, Department of Medicine - UC San Diego School of Medicine, 9500 Gilman Dr., La Jolla, CA 92093, 7. Helen Diller Family Comprehensive Cancer Center – UC San Francisco School of Medicine, 1450 3rd St, San Francisco, CA 94158, 8. Department of Pathology and Laboratory Medicine - UC Davis Comprehensive Cancer center, UC Davis school of Medicine, 2279 45th Street, Sacramento, CA 95817

† corresponding author: Olivier Harismendy: oharismendy@ucsd.edu

Abstract

Background: Systematic cancer screening has led to the increased detection of pre-malignant lesions (PMLs). The absence of reliable prognostic markers can lead to inadequate treatment resulting in unnecessary stress or avoidable progression. Importantly, most mutational profiling studies have relied on PML synchronous to invasive cancer, or performed in patients without outcome information, hence limiting their utility for biomarker discovery. The limitations in comprehensive mutational profiling of PMLs are in large part due to the significant technical and methodological challenges: most PML specimens are small, fixed in formalin and paraffin embedded (FFPE) and lack matching normal DNA.

Methods: Using test DNA from a highly degraded FFPE specimen, multiple targeted sequencing approaches were evaluated, varying DNA input amount (3-200 ng), library preparation strategy (BE: Blunt-End, SS: Single-Strand, AT: A-Tailing) and target size (whole exome vs cancer gene panel). Variants in high-input DNA from FFPE and mirrored frozen specimens were used for PML-specific variant calling training and testing, respectively. The resulting approach was applied to profile and compare multiple regions micro-dissected (mean area 5 mm^2) from 3 breast ductal carcinoma in situ (DCIS).

Results: Using low-input FFPE DNA, BE and SS libraries resulted in 4.9 and 3.7 increase over AT libraries in the fraction of whole exome covered at 20x (BE:87%, SS:63%, AT:17%). Compared to high-confidence somatic mutations from frozen specimens, PML-specific variant filtering increased recall (BE:79%, SS:74%, AT:62%) and precision (BE:87%, SS:88%, AT:80%) to levels expected from sampling variation. Copy number alterations were consistent across all tested approaches and only impacted by the design of the capture probe-set. Applied to DNA extracted from 9 micro-dissected regions (8 PML, 1 normal epithelium), the approach achieved comparable performance, identified candidate driver events (gains of *ERBB2* or *FGFR1*, loss of *TP53*) and illustrated the adequacy of the data to identify candidate driver mutations and measure intra-lesion genetic heterogeneity.

Conclusion: The approach presented enables mutational profiling from archived micro-dissected PML regions, supporting the identification of pre-malignant drivers, and the characterization of PML molecular heterogeneity and evolution, all critical milestones the development of biology-informed prognostic markers and precision chemo-prevention strategies.

Keywords: Targeted sequencing, cancer progression, pre-malignant lesion, variant calling, FFPE, micro-dissection, breast DCIS

Background

For some cancer types, the wide-spread adoption of cancer screening has increased the detection of pre-malignant lesions (PML) [1]. Today, breast ductal carcinoma in situ (DCIS) comprises nearly ~20% of all breast cancer diagnoses in the United States [2]. In the case of DCIS, disease-specific guidelines recommend surgical excision and sometimes systematic therapy. While treatment reduces the rate of second breast lesions diagnosis, it has not translated into increased survival rates suggesting overtreatment of PML and highlighting a critical need to improve risk models and identify prognostic markers [1,3,4]. Current PML risk models rarely account for molecular biomarkers such as mutations or copy number alterations, which are seldom profiled. This is in large part due to technical challenges in profiling PML: specimens from PML biopsies are typically formalin fixed and paraffin embedded (FFPE) in their entirety, to verify absence of any invasive component. As a consequence, no fresh or frozen material is available for research. Moreover, many PMLs observed in absence of invasive lesions are very small, sometimes less than a millimeter in diameter or containing fewer than 1000 cells. Hence, while FFPE specimens have successfully been used in high-throughput sequencing, the challenges posed by excessive formalin-induced deoxyribonucleic acid (DNA) damage – detailed below - are typically overcome by an increase in DNA input quantity [5–9], a solution not available for archival PML profiling. Thus, small FFPE PML specimens pose significant challenges in the generation of high throughput sequencing libraries and preclude the investigation of genetic biomarkers. To overcome these limitations, previous studies have been performed in fresh PML from areas adjacent to invasive disease instead of on pure PML, ignoring the vast majority of PML that are less likely to progress [10–15]. Profiling of pure PML in the absence of invasive disease is required to avoid such biases and thus necessitates methodology to work with archival FFPE specimens.

One of the main challenges of library preparation from damaged, low input DNA samples is to preserve the library complexity: the faithful and unbiased representation of all fragments in the starting DNA sample. Indeed the multiple steps of the library preparation, including the repair of the input DNA, the ligation of adapter, target enrichment and the multiple rounds of purification and PCR amplification can all act as bottlenecks, and introduce strong skews that will reduce the library complexity and eventually impact precision and recall of variant calling. Moreover, formalin is known to create adducts in the DNA and lead to spurious substitutions, which can be difficult to distinguish from true somatic variants, especially at low allelic fractions [16,17].

Finally, the most insightful prognostic biomarker studies of PML progression require long follow up to rely on actual outcome (recurrence, second events, survival) rather than proxy risk markers (grade, subtype, histological markers). As a consequence, most studies are retrospective and rely on old archived material without matching germline DNA sample, rendering the identification of high confidence somatic mutations more difficult. Hence, both technical and experimental challenges are hampering progress in PML mutational profiling.

Here we present the development of DNA library preparation and variant calling strategies specifically optimized for low abundance, damaged DNA, commonly extracted from PMLs. Using highly damaged DNA, we compared the effect of the input amount, the size of the captured genomic region, and library preparation strategy on the quality of coverage depth and breadth. We determined that library preparation using blunt-end (BE) adapter ligation strategy maximizes the library complexity down to 3 nanograms (ng) of input DNA and is compatible with whole exome capture. Using a set of DNA variants called from a frozen mirrored tissue specimen, we optimized the variant calling strategy to maximize its accuracy. We further demonstrated its validity on 10 DNA samples extracted from laser capture micro-dissected regions of PML or adjacent normal from DCIS of 3 independent patient FFPE specimen. We illustrate the utility of the approach to identify somatic mutations in candidate genes and characterize PML clonal heterogeneity within a specimen.

Methods

Sample collection and preparation

Test specimen: Mirrored frozen – FFPE tissue specimen from a HER2 positive invasive breast cancer was obtained from Asterand Biosciences (Detroit, MI). *DCIS specimen*: FFPE blocks were obtained from UCSD Health Anatomic Pathology after surgical biopsy, excision or mastectomy. The UCSD institutional review board approved the retrospective study and waived the requirement for consent. Consecutive sections of the blocks were used for Hematoxylin-Eosin staining (N=1; 4 μM glass slide) then for Laser Capture Microdissection (LCM; N=3; 7 μM glass slide coated with polyethylene naphthalate – ThermoFisher #LCM0522). The slides were stored at -20ºC in an airtight container with desiccant until ready for dissection (1 day to 3 months). The LCM sections were thawed and stained with eosin, sections were kept in xylene and dissected within 2 hours of staining. Laser Capture Microdissection was performed using the Arcturus Laser Capture Microdissection System. Matching regions from 3 adjacent sections were collected on one Capsure Macro Cap (Thermofisher), region size permitting. Post-dissection, all caps were covered and stored at -20ºC. *DNA extraction and QC:* The DNA was extracted from FFPE tissue using the QIAamp DNA FFPE tissue kit and QIAamp DNA Micro Kit (Qiagen) for the test specimen or LCM specimen, respectively. For the LCM sample, the membrane and adhering tissue were peeled off the caps using a razor blade and the peeled membrane was incubated in proteinase K digestion reaction overnight for 16 h at 56°C to maximize DNA yield after cell lysis and the elution was done in 20 μL. The extracted DNA was quantified by fluorometry (HS dsDNA kit Qbit – Thermofisher). All samples used in the study are described in Additional file 1: Table S1.

Targeted sequencing

DNA fragmentation: DNA was sheared down to 200 base pairs (bp) using Adaptive Focused Acoustics on the Covaris E220 (Covaris Inc) following manufacturer recommendations with the following modifications: 50 μL of Low TE buffer in microTUBE-130 tubes (AT libraries) or 10 μL Low EDTA TE buffer supplemented with 5 μL of truSHEAR buffer using a microTUBE-15 (SS and BE libraries).

Library preparation: AT libraries were prepared with the SureSelect XT HS protocol (Agilent Technologies) extending the adapter ligation time to 45 minutes (min). After ligation, excess adapters were removed using a 0.8x SPRI bead clean up with Agencourt AMPure XP beads (Beckman Coulter), then eluted into 21 µL of nuclease-free water. SS libraries were prepared using the Accel-NGS 1S Plus DNA Library Kit (Swift Biosciences). Prior to the single-strand ligation protocol, 15 µL of fragmented DNA was denatured at 95°C for 2 min, then set on ice. The adaptase and extension steps were performed by kit specifications followed by a purification step using 1.2x AMPure XP, eluted into 20 µL of nuclease free water. The subsequent ligation step incorporates SWIFT-1S P5 and SWIFT-1S P7 adapters, followed by a 1x AMPure XP bead clean-up and elution into 20 µL of nuclease free water. BE libraries were prepared using the Accel-NGS 2S PCR-Free DNA Library Kit (Swift Biosciences). Repair I was followed by a 1x AMPure bead cleanup, Repair II was followed by a 1x PEG NaCl cleanup, and Ligation I (P7 index adapter) and Ligation II (P5 UMI adapter) were followed by a 0.85x PEG NaCl cleanups. Only Ligation II cleanup was eluted into 20 µL Low EDTA TE, the other cleanups proceeded directly into the next reaction. Adapters used in the study are summarized in Additional file 1: Table S2.

Pre-Capture PCR amplification: Ligated and purified libraries were amplified using KAPA HiFi HotStart Real-time PCR 2X Master Mix (KAPA Biosystems). AT libraries were amplified with 2 µL of KAPA P5 primer and 2 µL of SureSelect P7 Index primer. SS libraries were amplified with 5 µL of SWIFT-1S P5 Index and P7 Index primers. BE samples were amplified with 5 µL of KAPA P5 and KAPA P7 primers. The reactions were denatured for 45 seconds (sec) at 98°C and amplified 13-15 cycles for 15 sec at 98°C, for 30 sec at 65°C, and for 30 sec at 72°C, followed by final extension for 1 min at 72°C. Samples were amplified until they reached Fluorescent Standard 3, cycles being dependent on input DNA quantity and quality. PCR reactions were then purified using 1x AMPure XP bead clean-up and eluted into 20 µL of nuclease-free water. The resulting libraries were analyzed using the Agilent 4200 Tapestation (D1000 ScreenTape) and quantified by fluorescence (Qubit dsDNA HS assay). Primers used in the study are summarized in Additional file 1: Table S2.

Targeted Capture Hybridization and Post-Capture PCR: Samples were paired and combined (12 µL total) to yield a capture “pond” of at least 350 ng, and supplemented with 5 µL of SureSelect XTHS and XT Low Input Blocker Mix. The baits for target enrichment consisted of either Agilent SureSelect Clinical Research Exome panel (S06588914), Human All Exon V7

panel (S31285117) or Cancer All-In-One Solid Tumor (A3131601). The hybridization and capture was performed using Agilent SureSelect XT HS Target Enrichment Kit following manufacturer's recommendations. Post-capture amplification was performed on the beads in a 25 µL reaction: 12.5 µL of nuclease-free water, 10 µL 5x Herculase II Reaction Buffer, 1 µL Herculase II Fusion DNA Polymerase, 0.5 µL 100 millimolar (mM) dNTP Mix and 1 µL SureSelect Post-Capture Primer Mix. The reaction was denatured for 30 sec at 98°C, then amplified for 12 cycles of 98°C for 30 sec, 60°C for 30 sec and 72°C for 1 min, followed by an extension at 72°C for 5 minutes and a final hold at 4°C. Libraries were purified with a 1x AMPure XP bead clean up and eluted into 20 µL nuclease free water in preparation for sequencing. The resulting libraries were analyzed using the Agilent 4200 Tapestation (D1000 ScreenTape) and quantified by fluorescence (Qbit – ThermoFisher)

Sequencing: All libraries were sequenced using on the HiSeq 4000 sequencer (Illumina) for 100 cycles in Paired-End mode. Libraries with distinct indexes were pooled in equimolar amounts. The sequencing and capture pools were later deconvoluted using program bcl2fastq.

Data analysis

Sequencing reads processing and coverage quality control: Sequencing data was analyzed using bcbio-nextgen (v1.1.6) as a workflow manager [18]. Samples prepared with identical targeted panels were down-sampled to have equal number of reads using seqtk sample (v1.3) [19]. Adapter sequences were trimmed using Atropos (v1.1.22), the trimmed reads were subsequently aligned with bwa-mem (v0.7.17) to reference genome hg19, then PCR duplicates were removed using biobambam2 (v2.0.87) [20–22]. Additional BAM file manipulation and collection of QC metrics was performed with picard (v2.20.4) and samtools (v1.9) [22]. The summary statistics of the sequencing and coverage results are presented in Additional file 1: Table S3.

Copy number analysis: Copy number alterations (CNAs) were called using CNVkit (v0.9.6) [23] using equal sized bins of ~250 bp. Any bins with $\log_2$ copy ratio lower than -15, were considered artifacts and removed. Breakpoints between copy number segment were determined using the circular binary segmentation algorithm ($p < 10^{-4}$)[24]. Low quality segments were removed from downstream analysis (less than 10 probes, biweight midvariance more than 2 or $\log_2$ copy ratio confidence interval contains 0). Copy number genomic burden was computed as the sum of sizes

of segments in a gain ($\log_2$(ratio)>0.3) or loss ($\log_2$(ratio)<-0.3) over the sum of the sizes of all segments. The summary statistics of CNA calling on the test specimen are reported in Additional file 1: Table S4. Chromosomal arm gains and losses were called when more than half their total length was involved in a gained and lost segment, respectively. Gene copy number estimates were assigned based on the segment that covered the gene. For the *test specimen*, if more than one segment covered a gene then the higher confidence segment was used. For the *DCIS specimen* copy number alterations were determined for all autosomal genes containing at least 3 bins whose segments were covered by at least 110 probes (N=17,750 total). Additionally, due to the imprecision of segmentation breakpoints, any genes with a breakpoint identified in one region of a patient, were removed from the comparison to other regions. Loss of heterozygosity (LOH) was called for segments with B-allele frequencies lower than 0.3 or greater than 0.7.

Variant calling and initial filtering: Single nucleotide variants (SNVs) and short insertions and deletions (indels) were called with VarDictJava (v1.6.0) and Freebayes (v1.1.0.46) [25,26]. Variants were required to fall within a 10 bp boundary of targeted regions that overlapped with RefSeq genes. Only variants called by both algorithms were considered. These ensemble variants were then subjected to an initial filtering step with default bcbio-nextgen tumor-only variant calling filters listed in Additional file 1: Table S5. Functional effects were predicted using SnpEff (v4.3.1) [27]. The resulting variants are referred to as raw ensemble variants.

Germline variant filtering: In absence of a matched normal control for both test (frozen and FFPE) and DCIS specimens, somatic mutations were prioritized computationally using the approach from the bcbio-nextgen tumor-only configuration then additionally subjected to more stringent filtering [28]. Briefly, common variants (MAF>10^{-3}) present in population databases - 1000 genomes (v2.8), ExAC (v0.3), or gnomAD exome (v2.1) - were removed unless in a tier 1 gene from the cancer gene consensus and present in either COSMIC (v68) or clinvar (20190513) [18,29–33]. Additionally, variants were removed as likely germline if found at a variant allelic fraction (VAF) greater or equal to 0.9 in non-LOH genomic segments – as determined by CNA analysis (above). The remaining variants are referred to as candidate somatic mutations.

Analysis specific filtering of candidate somatic mutations: Additional filtering was implemented in a context specific to the analysis presented. *1) Calling "gold standard" mutations from the frozen test specimen:* the candidate somatic mutations in the DNA of the frozen test specimens were

filtered for high-quality variants: ensemble quality score greater than 175, average number of read mismatches less than 2.5, position covered by at least 25 reads, mean position in read greater than 20, microsatellite length less than 5, and VAF more than 0.15. This resulted in 138 SNVs and 10 indels. 2) *Benchmarking mutations in FFPE test specimens*: mutations in the DNA of the FFPE test specimens required specific filtering due to the abundant low-frequency damage as well as lower coverage depth. The following parameters were used: position covered by at least 5 reads, mean position in read greater than 15, number of average read mis-matches less than 2.5, Fisher strand bias p-value greater than 0.1, microsatellite length less than 5, and VAF more than 0.15. The accuracy of resulting DNA variants from the test FFPE specimen was measured against the set of "gold standard" variants from the mirrored frozen specimen using vcfeval by RTG-tools (v3.10.1), using variant ensemble quality as the score [34]. The results of the benchmarking analysis are reported in Additional file 1: Table S6. 3) *Profiling dissected regions from the DCIS specimen:* in addition to the filtering of FFPE candidate somatic mutations presented above, the following steps were implemented. Any variants found at high VAF (>0.9) in non-LOH segments in one region were also excluded from the variants from all other regions of same patient. Candidate somatic mutations with ensemble quality score lower than 115 were excluded, corresponding to the optimal F-score obtained for low-input BE libraries in the benchmarking analysis. To the exception of few well-described hotspot mutations in breast cancer (*PIK3CA, TP53, GATA3*), somatic mutations identified in more than one patient were removed.

Clonality analysis: To allow the analysis of clonal relationships between regions of the same patient, the coverage depth of each allele at any remaining mutated position in any region was extracted using Mutect2 joint variant caller on the sets of aligned reads from each region. In order to call a mutation either absent or present in a region, we used a Bayesian inference model specifically designed for multi-region variant calling [35]. Treeomics (v1.7.10) was run with the default parameters except for e=0.02.

Results

Evaluation of targeted sequencing approaches for low input FFPE DNA

Regions of PMLs on a histological section can contain as few as 500 cells, corresponding to 3.3 ng of haploid DNA. The expected reduced DNA extraction yield can be mitigated by combining regions matched across sequential sections. Hence, optimizing targeted sequencing using 3 to 10 ng of input DNA is a reasonable objective to identify high confidence mutations in PML. To develop the methodology, a test DNA sample was extracted from a 4 year-old FFPE HER2 positive breast invasive carcinoma which showed significant fragmentation (DNA integrity number of 2.4), likely representative of DNA extracted from old archived specimens. A high-throughput sequencing library was prepared from decreasing amount of input DNA (200, 50 or 10 ng) using traditional A-tailing adapter ligation protocol optimized for low-input, damaged DNA (referred to as AT method - Figure 1A). After capture of the whole-exome by hybrid selection, the DNA libraries were amplified and sequenced. The performance was evaluated in comparison to whole exome data generated from 200 ng of DNA extracted from a mirrored frozen tissue specimen [36]. Libraries generated from 200 or 50 ng FFPE DNA achieved reasonable coverage, with nearly all targeted bases covered at least 20 fold (referred to as Cov20). In contrast, the sequencing libraries from 10 ng FFPE DNA lacked complexity (79% read PCR duplicates), resulting in 17% Cov20 after elimination of the duplicate reads (Figure 1B-C). Importantly, targeting the sequencing to a restricted cancer gene panel (710 kb total size) did not improve this result, as the 3 ng libraries had a high percentage of duplicate reads (83%) and 1.6% Cov20 (Figure 1D-E). This result suggests that the bottleneck reducing the library complexity originates upstream of the targeted capture, which led us to examine the initial ligation of the sequencing adapters.

Library preparation methods which utilize alternate ligation techniques have previously been shown to increase the complexity of the library notably for the analysis of cell free DNA [37,38], ancient DNA [39–41] and other applications [42,43]. We therefore evaluated blunt-end ligation (BE) and single strand ligation (SS) library preparation strategies to increase the number of input DNA fragments incorporated in the library and enhance the resulting complexity and usable sequence coverage (Figure 1A, Additional file 2: Figure S1). The cancer panel capture of BE libraries prepared from 3 ng of test DNA showed a reduced percentage of duplicate reads compared to low input AT libraries (73% vs 83% respectively Figure 1E), leading to a dramatic

increase in Cov20 (99.7% vs 2%) and bringing it to levels comparable to high input (50 ng) AT libraries (Figure 1D). In turn, the SS library offered a lesser, but measurable, improvement over AT library for low input (Figure 1D-E). The superiority of the BE and SS strategies were further confirmed using whole exome capture with BE and SS libraries resulting in 84% and 63% Cov20 at low input (3 ng), respectively, higher than 17% observed for low input (10 ng) AT libraries (Figure 1B). Compared to the cancer panel capture, the improvements of these alternative ligation strategies on whole exome sequencing were milder but remained remarkable and, in the case of BE strategy, likely to support more sensitive mutational profiling of archived PMLs.

Somatic mutation profiling from low input FFPE DNA

At a minimum, both SNVs and indels are necessary to evaluate the mutational landscape of PML. Unfiltered SNVs identified in FFPE DNA showed both a high overall abundance (422,322) of low variant allelic fraction substitutions (VAF <5%) and bias of C to T substitutions (53%), which is expected from the cytosine deamination resulting from formalin fixation [16,17]. In contrast, low VAF variants from frozen DNA were much lower in abundance (175,364) but contained a high-prevalence (52%) of C to A substitutions consistent with previously reported 8-oxoguanine damage observed in frozen samples (Additional file 2: Figure S2) [44]. We hypothesized that we could discriminate against artifactual FFPE variants in the test specimens using stringent filtering criteria including high strand bias, low allelic fraction and poor concordance between multiple variant callers in order to call accurate somatic variants in FFPE preserved PML (Methods).

First, we established a set of benchmarking somatic mutations from the test DNA extracted from a mirroring frozen tissue specimen [36]. Its whole exome sequence resulted in 138 SNVs and 10 indels that were used to measure performance of the variant calling from the FFPE libraries generated above. Prior to filtering, the analysis of variants from low input AT libraries resulted in an average of 5,148 false positive somatic mutations. In contrast, the analysis of variants from BE and SS libraries resulted in an average of 332 and 1,365 false positive mutations, respectively (Figure 2A). We developed additional filtering criteria, trained on variants from the high-input (200 ng) FFPE library. These additional filters considerably reduced the fraction of false positives (Figure 2B), increasing precision from less than 30% to 80%, 87% and 88% for the AT, BE and SS low input libraries, respectively (Figure 2C-D). The variant recall increased

from 62% to 79% and 74% for the AT, BE and SS low-input libraries, respectively, consistent with differences observed in Cov20 (Additional file 1: Table S6). Notably, the resulting accuracy is in line with the one obtained with variants called using sub-sampled data from the frozen specimen (87% precision, 80% recall), indicating that the differences mainly comes from sampling rather than from technical artifacts. The improvement in accuracy was similar for the small number of indels (Additional file 1: Table S6). These data suggest that FFPE specific filtering of ensemble variant calls paired with BE library preparation enables accurate clonal somatic SNV and indel variant calling of whole exome sequencing data from 3 ng FFPE test DNA.

In contrast to SNVs and indels, Copy Number Alterations (CNA) can be accurately identified using lower coverage depth whole genome sequencing data, though has been more challenging in targeted sequencing [45,46]. We evaluated the ability of all input quantity and library preparation methods to reliably identify CNA (Methods). The genome-wide CNA burden obtained from low input SS and BE library was consistent with the one of high-input (200 ng) AT libraries (8.1%, 7% and 8.4% respectively – Figure 2E and Additional file 1: Table S4), while it was underestimated from the low input AT library (5.7%). Interestingly, this difference is not observed using the results of the cancer panel sequencing (Figure 2F) likely due to differences in probe density between the two capture designs (below). The resulting level of copy number gains and losses estimated for each chromosome arms and more focal areas were highly reproducible between all tested library preparation strategies (Additional file 2: Figure S3-S4). Additionally, the copy number status of known cancer genes was also consistent between exome and cancer panel, including the expected *ERBB2* amplification which was correctly determined in all cases. In a few instances, the denser tiling of the exome probes helped identify a copy number breakpoint missed in the cancer panel, resulting in discordant copy number estimate for a few genes (Additional file 2: Figure S5). This suggests that the input amount and quality of the sample has little impact on the accuracy of the copy number profiling, albeit this observation was limited to a specimen with few CNAs.

Mutational profiling of breast PML

To validate the optimized targeted sequencing and somatic variant calling on PMLs, we collected archived tissue specimens from 3 patients diagnosed with breast ductal carcinoma in situ (DCIS – 1 low grade, 2 high grade) without evidence of invasive disease. A total of 8 PML

regions and one normal breast epithelium region (patient 3, region 3N) were isolated by laser capture microdissection (LCM – Figure 3A). The dissected regions had a mean area of 5 mm^2 and, combined over three adjacent sections, contained an average of 80,000 cells (Figure 3B). For one large DCIS region, adjacent sections (patient 2, regions 2A1 and 2A2) were processed independently for replication. For each region, between 1.4 and 21 ng of DNA were extracted and used to prepare exome libraries using the BE method. The rate of duplicate reads was between 32 and 82%, and, as expected, inversely correlated with the amount of input DNA (Additional file 2: Figure S6). The resulting mean coverage depth was comprised between ~2 and 45 fold, which is sufficient for accurate detection of CNA, but likely limiting the sensitivity to identify mutations, particularly in patient 2.

Between 7% and 43% of the regions' genomes were involved in CNAs, predominantly through copy number losses (Figure 4A). With the exception of region 2B, the CNA burden was consistent between regions of the same patient and minimal in normal breast epithelium (<5%). A total of 18 chromosome arms were affected by copy number changes in at least one DCIS region. None of these were altered in the normal breast epithelium (Figure 4B). Some of the chromosome arm losses identified, such as 6q, 8p, 16q, 17p or 22q are frequent in DCIS [47]. Within patient 1 and 3, all regions have consistent CNA suggesting a common clonal ancestor. In contrast, regions 2A and 2B have different number of arms altered (5 vs 13, respectively) with only 3 in common. Both regions featured high nuclear grade, but only 2B showed comedo-necrosis, a marker of more advanced and worse prognosis DCIS. Region 2B was the only region affected by chromosome arm gains at 8q, 20q and 21q. The absence of these gains in 2A as well as its additional losses of 4p and 9p, suggest the independent clonal evolution of 2A and 2B. Finally, all PML regions from patient 2 and 3 displayed a loss of 17p, generally associated with *TP53* loss of heterozygosity (LOH) frequently observed in high-grade specimens. At a higher resolution, out of 98 cancer genes evaluated, 38 had a CNA in at least one region (Figure 4C). The most notable ones were the amplification of *ERBB2* in all regions of patient 2, amplification of *FGFR1* in all regions of patient 3 and loss of *TP53* in patient 2 and 3. This latter observation was consistent with 17p LOH and confirmed by change in B-allele frequency at heterozygous SNPs (Additional file 2: Figure S7). Similar to chromosome arms, none of the genes were altered in the normal epithelium and most had consistent copy numbers between regions of the same patient, with the exception of 12 genes distinguishing regions 2A and 2B and further supporting separate clonal evolution.

We next identified somatic mutations in each region of patient 1 and 3's specimens. After additional quality filtering using cross-patient information, we identified between 9 and 65 somatic mutations per PML region, of which 5 to 41 were non-silent (Additional file 1: Table S7). The resulting mutational burden (0.51 - 1.84 mutations/Mb) is slightly lower than for invasive breast cancer [48]. None of the somatic mutations identified were well-known actionable mutations in cancer despite most cancer genes and hotspots being adequately sequenced in at least one region of each patient (Additional file 1: Table S8) [49]. The somatic mutations were then used to characterize the clonal relationships between regions. To account for uneven sequencing coverage between regions and the possibility of random allelic dropout, we used a maximum likelihood approach, comparing allelic fraction and total read depth of any mutated position in all regions of patients 1 and 3 (Figure 4D-E) [35]. Mutations in patient 1 were evaluated at 57 mutated positions, 50 of which are confidently identified in all 3 regions. While a portion of these may be residual germline variants, 3 mutations resembled cancer driver mutations found in *FAT1*, and *PRDM1* (Additional file 1: Table S9). The coverage depth of the remaining variants is too low in 1 or 2 regions to confidently determine their distribution. Mutations in patient 3 were evaluated at 84 positions, 66 of which were shared by all 4 regions and likely residual germline variants. The results were used to build a phylogenic tree illustrating the clonal relationship between regions (Figure 4F). Interestingly, region 3N is mutated at 3 positions not found in the PML regions. These could represent mutations acquired in aging normal tissue or residual germline variants lost in the PMLs. The 3 PML regions gained an additional 9 mutations before diverging, each gaining between 1 and 3 mutations that were not shared. Importantly, and in contrast to the result of the copy number analysis, none of the somatic mutations identified in any patient were common drivers of breast cancer. Nevertheless, an *ERBB3 Ile763Leu* substitution was exclusively observed in all 3 PML regions of patient 3. This mutation is predicted to be deleterious, possibly activating this uncommon driver of breast cancer [50,51] and may have contributed, in concert with *FGFR1* gain, to the clonal expansion observed in this patient. Overall, our analysis suggests that even in absence of normal DNA, and akin to experiments in large tumors, variants from multi-region sequencing can be used to trace evolutionary relationships between areas of pre-malignancy [35,52].

Discussion

The results presented here demonstrate our ability to perform comprehensive mutational profiling from some of the most challenging clinical specimens with DNA in limited quantity – down to 3 ng - and of poor quality - highly degraded and chemically altered. In particular, this demonstration relied on a thorough benchmarking study using DNA from mirrored matching frozen vs FFPE specimens, which provided a real-world experimental framework to guide the process development.

We demonstrated that by utilizing a sequencing library preparation that uses a non-standard adapter ligation, we can drastically improve sequencing performance from these challenging specimens. A-tailing, together with transposon-mediated construction, is one of the most popular methods to prepare high-throughput sequencing libraries. While the latter necessitates longer DNA fragments and is not-suitable for highly degraded DNA, A-tailing has been broadly used in library preparation and is compatible with highly degraded specimens so long as DNA input is increased. We illustrated this limitation, analyzing targeted sequencing from limited dilutions and saw a drop in coverage and variant calling accuracy below 50 ng DNA input. Target coverage cannot be rescued by sequencing of a smaller panel, since the bottleneck resulting in lack of library complexity occurs prior to capture. For clinical reasons, to allow the thorough inspection of all tissue parts to formally exclude invasive disease, all pure PMLs are fixed in formalin and archived. Furthermore, areas of PML are typically small, limiting the quantity of material available for analysis. For the largest lesions, a labor-intensive dissection and pooling can increase the amount of DNA extracted but would preclude the study of their genetic heterogeneity. Similar to the benefit demonstrated on ancient DNA [39,41], we showed that an alternative library preparation using either single-strand and even more so for blunt-end ligation strategies considerably improved both coverage and consequently variant calling performances. Despite the recognized high efficiency of sticky-end ligation, end-repair and addition of an overhanging adenosine is likely the rate-limiting step on highly damaged DNA.

Another challenge we faced and addressed was calling mutations in absence of a matching normal DNA in both the test and PML DNA, likely leading to some ambiguous mutation classification [53]. The most useful PML specimens for biomarker studies are the ones with long follow-up, and aside from logistical challenges of collecting matching blood or saliva as part of routine clinical workflow, these traditional sources of normal DNA are generally not available for

archival PML. The dissection of adjacent normal tissue, performed for one specimen in this study, can be sometimes used. While sufficient material can be found at the margin of the surgical specimen, the cellularity of the normal tissue will vary greatly between organs and histological context leading to even smaller quantities of DNA. In the breast, the normal ductal tree is poorly cellular in comparison to dysplastic and in situ proliferative lesions. In some instances, an area of high lymphocytic infiltration, for example at the location of a previous biopsy, can be used. Such histologically normal tissue are also formalin fixed and their mutational profiling presents similar, if not more, challenges than for PMLs. Furthermore, and as demonstrated elsewhere, some histologically normal specimens will contain a few somatic mutations at low-allelic fraction, resulting from early clonal selection, such as the few private mutations identified in sample 3N [54,55]. Nevertheless, the inclusion of such a matched normal DNA in the analysis and interpretation would greatly aid in the removal of residual germline DNA and additional sequencing artifacts. In absence of matching normal DNA, the parallel sequencing of a panel of unmatched normal DNA, from the same ethnic background and processed using the exact same protocol and analysis is recommended, especially in a clinical setting [53]. This was not available for this benchmarking study. Instead, we filtered common variants using public databases following recommendation provided elsewhere [28,56]. This approach will miss rare germline variants, especially present in rare, or under-studied ethnicities. Previous studies have observed that tumor-only exomes may lead to ~300 residual germline variants after careful filtering [53,57]. Importantly, coding and deleterious germline variants could be a source of false positives. In our study, multi-region sampling provided additional information to help us classify mutations, and we determined that 50-66 mutations were shared and likely represented residual germline variants. This approach would however not remove the ambiguity for shared mutations and, in the event this mutation is an oncogenic driver common to all regions, additional validation steps may be required, including sequencing from a more distant region located on a separate tissue block, or comparison to its allelic fraction and copy number status in the bulk DNA.

Independent of the possible residual germline variants, we took specific steps to benchmark variant calling in highly degraded FFPE DNA, comparing the results to high quality variants called from the DNA of an adjacent frozen specimen. After carefully down-sampling the data to obtain the same number of raw sequencing reads – including *in silico* “replicates” from the deeper reference (frozen tissue) dataset itself - we identified two main mode of errors. First, a large number of false negative variants, leading to lower recall, were directly associated to the

uneven and lower coverage depth, particularly in the low input FFPE AT library. The high and more even coverage observed in the BE libraries, for the same number of raw reads, remediated this issue, resulting in recall similar to the one expected from sampling bias observed in other studies [58]. Second, the false positives were mostly due to C to T substitutions as a consequence of formalin fixation, as previously observed. Such substitutions however remained at low allelic fraction and displayed strong strand bias, which could be remediated using stringent heuristic filtering. Alternate solutions have been described elsewhere to remove same or similar sequencing artifacts using machine learning [59] or relying on the precise substitution signature of the artifacts [60,61]. These would likely yield similar or superior results. DNA damage can also be repaired prior to library preparation altogether using cocktails of DNA repair enzymes, such as UDG and Fpg [62,63]. This strategy would decrease false positive mutations [64] but typically require more than 5 ng FFPE DNA and the extra enzymatic step would likely add bottleneck and decrease library complexity.

Of the 3 DCIS patients studied, all displayed chromosomal copy number changes previously observed in DCIS, leading to losses of known tumor suppressors (*TP53*) or gains of known oncogenes (*ERBB2* or *FGFR1*). In contrast, as observed in 2/3 patients, we observed fewer somatic mutations than previously observed [65], perhaps consistent with the lower nuclear grade of the regions studied. Additionally, none of the somatic mutations were known or likely cancer driver mutations. Neither the lower mutation burden nor the lack of known breast cancer driver mutations were surprising, as these specimens represent pure DCIS lacking any invasive component, and thus should bear less genomic resemblance to breast cancer [65]. The relative contribution of gene copy number alterations vs somatic mutations to cellular proliferation and clonal selection in normal and pre-malignant tissue is an active field of study [54,55,66] and progress in this field will require multi-modal molecular profiling approaches compatible with small amounts of archived tissue, such as the one described here.

Beyond the identification of drivers of growth and proliferation, the proposed approach can help measure the genetic heterogeneity in PML lesions. In breast DCIS, phenotypic heterogeneity associated with subtype and grade can co-exist within a specimen [67]. Additionally, immunostaining of key markers has revealed spatial heterogeneity within a duct and between ducts of a patient [68]. But the mutational landscape underlying such heterogeneity has not been thoroughly studied in pure DCIS at a genome-wide level for the technical reasons mentioned herein. Multi-region assessment of karyotypes, select gene copy number [69] and

mitochondrial mutations [70] suggested significant heterogeneity in DCIS but its clinical significance and association with other progression risk factors has not been assessed. Copy-number heterogeneity has also been observed via single-cell sequencing from frozen DCIS patient specimens, albeit in the presence of an invasive lesion [15]. A similar approach has been developed in archived tissue specimens, but none have been used in large studies or in pure DCIS [71] . While single-cell sequencing may be able to scale up – both number of cells and number of samples, it cannot yet identify point mutations with high sensitivity. Hence, in the context of a clinical study, multi-region sequencing enabled by LCM may be preferable as it would increase the accuracy of the clonal evolution and enable the identification of driver mutations and mutational signatures [72]. Moreover, the results of multi-region genomic profiling would enable us to place somatic mutations and copy number alterations in the context of the surrounding extra-cellular matrix or stromal composition obtained via imaging and morphological studies, providing a granular view of the premalignant landscape as aspired by the pre-cancer atlas [73].

Conclusions

We present both methodological and analytical advances enabling targeted sequencing from small, archived PML lesions. Specifically, we showed that blunt-end ligation of the sequencing adapter to the fragmented and damaged DNA was key to increasing the quality of the exome sequencing from a minute amount of DNA extracted from archived specimens. A subsequent multi-caller analysis strategy, complemented by dedicated filters, identified somatic mutations, eliminating false-positive and residual germline mutations - two critical hurdles in the mutational profiling of PML. Importantly, the approach was developed on real world samples using a well-characterized test sample and further validated on micro-dissected PML regions. These advances now enable mutational profiling of PML lesions, unlocking the untapped registry of archived PML specimens to comprehensively investigate their molecular heterogeneity and assess the contribution of somatic DNA alterations to cellular proliferation and progression to invasive cancer.

List of abbreviations

BE: Blunt-end
SS: Single-strand
AT: A-tailing
DCIS: Ductal carcinoma in situ
LCM: Laser capture microdissection
IDC: Invasive ductal carcinoma
FFPE: Formalin-fixed paraffin embedded
LOH: Loss of heterozygosity
VAF: Variant allelic frequency
PML: Pre-malignant lesion
CNA: Copy number alteration
Cov20: Fraction of base pairs covered at 20x or more

Declarations

Ethics approval and consent to participate: The retrospective use of clinical specimen was approved by the UC San Francisco Institutional Review Board and UC San Diego Institutional Review Board who granted a waiver of informed consent.

Consent for publication: Not applicable

Availability of data and materials: Configuration of bcbio pipeline is available publicly on GitHub: https://github.com/danielanach/bcbio-ffpe-no-normal-config/blob/master/bcbio_ffpe-no-normal.yaml. The raw sequencing data for the test specimen have been deposited with links to BioProject accession number PRJNA615755 in the NCBI BioProject database. The raw sequencing data from the DCIS patients has been deposited to the NCBI dbGaP (release pending).

Competing interests: None

Funding: This work is supported by funding from the National Institute of Health (U01CA196406, U01CA196406-03S1, R01DE026644 and T32GM008806), the National Cancer Institute (P30CA023100) and the California Tobacco Related Disease Research Program pre-doctoral fellowship to DN (28DT-0011).

Authors' contributions: SB and FH selected specimen and performed pathology annotation, EZ and TOK identified breast cancer patients and reviewed associated clinical data. JS prepared the DNA samples, KJ and HY performed the targeted sequencing. KJ, DN, OH designed the test study, OH, GH, LE, SB designed the validation study. DN and OH performed the analysis and wrote the manuscript. All authors approved the final manuscript.

Acknowledgements: We express our gratitude to members of the Moores Cancer Center Biotechnology and Tissue Technology Shared Resource: Drs Molinolo, Kaushal, Estrada and Kimberly McIntyre for their technical assistance. All sequencing was conducted at the IGM Genomics Center, University of California, San Diego, La Jolla, CA. Figure 3A was created using images from BioRender.com.

References

1. Esserman LJ, Thompson IM, Reid B. Overdiagnosis and overtreatment in cancer: An opportunity for improvement. JAMA - J Am Med Assoc. 2013;310:797–8.
2. Siegel RL, Miller KD, Jemal A. Cancer statistics, 2020. CA Cancer J Clin. 2020;70:7–30.
3. Marmot M, Altman DG, Cameron DA, Dewar JA, Thompson SG, Wilcox M. The benefits and harms of breast cancer screening: An independent review. Lancet. 2012;380:1778–86.
4. Bleyer A, Welch HG. Effect of three decades of screening mammography on breast-cancer incidence. N Engl J Med. 2012;367:1998–2005.
5. Menon R, Deng M, Boehm D, Braun M, Fend F, Boehm D, et al. Exome enrichment and SOLiD sequencing of formalin fixed paraffin embedded (FFPE) prostate cancer tissue. Int J Mol Sci. 2012;13:8933–42.
6. Hedegaard J, Thorsen K, Lund MK, Hein AMK, Hamilton-Dutoit SJ, Vang S, et al. Next-generation sequencing of RNA and DNA isolated from paired fresh-frozen and formalin-fixed paraffin-embedded samples of human cancer and normal tissue. PLoS One. 2014;9:e98187.
7. Allen EM Van, Wagle N, Stojanov P, Perrin DL, Cibulskis K, Marlow S, et al. Whole-exome sequencing and clinical interpretation of FFPE tumor samples to guide precision cancer medicine. Nat Med. 2014;20:682–8.
8. Munchel S, Hoang Y, Zhao Y, Cottrell J, Klotzle B, Godwin AK, et al. Targeted or whole genome sequencing of formalin fixed tissue samples: Potential applications in cancer genomics. Oncotarget. 2015;6:25943–61.
9. Astolfi A, Urbini M, Indio V, Nannini M, Genovese CG, Santini D, et al. Whole exome sequencing (WES) on formalin-fixed, paraffin-embedded (FFPE) tumor tissue in gastrointestinal stromal tumors (GIST). BMC Genomics. 2015;16:892.
10. Miron A, Varadi M, Carrasco D, Li H, Luongo L, Kim HJ, et al. PIK3CA mutations in in situ and invasive breast carcinomas. Cancer Res. 2010;70:5674–8.
11. Sontag L, Axelrod DE. Evaluation of pathways for progression of heterogeneous breast tumors. J Theor Biol. 2005;232:179–89.
12. Yates LR, Gerstung M, Knappskog S, Desmedt C, Gundem G, Van Loo P, et al. Subclonal diversification of primary breast cancer revealed by multiregion sequencing. Nat Med. 2015;21:751–9.
13. Newburger DE, Kashef-Haghighi D, Weng Z, Salari R, Sweeney RT, Brunner AL, et al. Genome evolution during progression to breast cancer. Genome Res. 2013;23:1097–108.
14. Oikawa M, Yano H, Matsumoto M, Otsubo R, Shibata K, Hayashi T, et al. A novel diagnostic

method targeting genomic instability in intracystic tumors of the breast. Breast Cancer. 2015;22:529–35.
15. Casasent AK, Schalck A, Gao R, Sei E, Long A, Pangburn W, et al. Multiclonal Invasion in Breast Tumors Identified by Topographic Single Cell Sequencing. Cell. 2018;72:205–17.
16. Arreaza G, Qiu P, Pang L, Albright A, Hong LZ, Marton MJ, et al. Pre-analytical considerations for successful next-generation sequencing (NGS): Challenges and opportunities for formalin-fixed and paraffin-embedded tumor tissue (FFPE) samples [Internet]. Int. J. Mol. Sci. 2016. Available from: http://dx.doi.org/10.3390/ijms17091579
17. Do H, Dobrovic A. Sequence artifacts in DNA from formalin-fixed tissues: Causes and strategies for minimization. Clin Chem. 2015;61:64–71.
18. Guimera RV. bcbio-nextgen: Automated, distributed next-gen sequencing pipeline. EMBnet.journal [Internet]. 2012;17:30. Available from: http://journal.embnet.org/index.php/embnetjournal/article/view/286
19. Li H. Seqtk. GitHub. 2015.
20. Didion JP, Martin M, Collins FS. Atropos: Specific, sensitive, and speedy trimming of sequencing reads. PeerJ. 2017;5:e3720.
21. Li H, Durbin R. Fast and accurate short read alignment with Burrows-Wheeler transform. Bioinformatics. 2009;25:1754–60.
22. Broad Institute. Picard tools [Internet]. https://broadinstitute.github.io/picard/. 2016. Available from: https://broadinstitute.github.io/picard/%5Cnhttp://broadinstitute.github.io/picard/
23. Talevich E, Shain AH, Botton T, Bastian BC. CNVkit: Genome-Wide Copy Number Detection and Visualization from Targeted DNA Sequencing. PLoS Comput Biol. 2016;2:e1004873.
24. Olshen AB, Bengtsson H, Neuvial P, Spellman PT, Olshen RA, Seshan VE. Parent-specific copy number in paired tumor-normal studies using circular binary segmentation. Bioinformatics. 2011;27:2038–46.
25. Lai Z, Markovets A, Ahdesmaki M, Chapman B, Hofmann O, Mcewen R, et al. VarDict: A novel and versatile variant caller for next-generation sequencing in cancer research. Nucleic Acids Res. 2016;44:e108.
26. Garrison E, Marth G. Haplotype-based variant detection from short-read sequencing. 2012 [cited 2020 Jan 20]; Available from: https://arxiv.org/abs/1207.3907
27. Cingolani P, Platts A, Wang LL, Coon M, Nguyen T, Wang L, et al. A program for annotating and predicting the effects of single nucleotide polymorphisms, SnpEff. Fly (Austin) [Internet]. 2012;6:80–92. Available from: http://www.tandfonline.com/doi/abs/10.4161/fly.19695

28. bcbio tumor-only. Available from: https://bcbio.wordpress.com/2015/03/05/cancerval/
29. 1000 Genomes Project Consortium. An integrated map of genetic variation. Nature. 2012;491:56–65.
30. Exome Aggregate Consortium. ExAC Browser. Online. 2016.
31. Karczewski KJ, Francioli LC, Tiao G, Cummings BB, Alföldi J, Wang Q, et al. Variation across 141,456 human exomes and genomes reveals the spectrum of loss-of-function intolerance across human protein-coding genes. bioRxiv. 2019;
32. Forbes SA, Beare D, Boutselakis H, Bamford S, Bindal N, Tate J, et al. COSMIC: Somatic cancer genetics at high-resolution. Nucleic Acids Res. 2017;45:D777–83.
33. Landrum MJ, Lee JM, Benson M, Brown GR, Chao C, Chitipiralla S, et al. ClinVar: Improving access to variant interpretations and supporting evidence. Nucleic Acids Res. 2018;46:D1062–7.
34. Cleary JG, Braithwaite R, Gaastra K, Hilbush BS, Inglis S, Irvine SA, et al. Joint variant and de novo mutation identification on pedigrees from high-throughput sequencing data. J Comput Biol. 2014;21:405–19.
35. Reiter JG, Makohon-Moore AP, Gerold JM, Bozic I, Chatterjee K, Iacobuzio-Donahue CA, et al. Reconstructing metastatic seeding patterns of human cancers. Nat Commun. 2017;8:14114.
36. Levy E, Marty R, Gárate Calderón V, Woo B, Dow M, Armisen R, et al. Immune DNA signature of T-cell infiltration in breast tumor exomes. Sci Rep. 2016;6:30064.
37. Troll CJ, Kapp J, Rao V, Harkins KM, Cole C, Naughton C, et al. A ligation-based single-stranded library preparation method to analyze cell-free DNA and synthetic oligos. BMC Genomics. 2019;20:1023.
38. Bennett CW, Berchem G, Kim YJ, El-Khoury V. Cell-free DNA and next-generation sequencing in the service of personalized medicine for lung cancer. Oncotarget. 2016;7:71013–35.
39. Bennett EA, Massilani D, Lizzo G, Daligault J, Geigl EM, Grange T. Library construction for ancient genomics: Single strand or double strand? Biotechniques. 2014;
40. Dabney J, Knapp M, Glocke I, Gansauge MT, Weihmann A, Nickel B, et al. Complete mitochondrial genome sequence of a Middle Pleistocene cave bear reconstructed from ultrashort DNA fragments. Proc Natl Acad Sci U S A. 2013;110:15758–63.
41. Gansauge MT, Meyer M. Single-stranded DNA library preparation for the sequencing of ancient or damaged DNA. Nat Protoc. 2013;8:737–48.
42. Sundaram AYM, Hughes T, Biondi S, Bolduc N, Bowman SK, Camilli A, et al. A comparative study of ChIP-seq sequencing library preparation methods. BMC Genomics. 2016;17:816.

43. Ma S, Hsieh YP, Ma J, Lu C. Low-input and multiplexed microfluidic assay reveals epigenomic variation across cerebellum and prefrontal cortex. Sci Adv. 2018;4:eaar8187.
44. Costello M, Pugh TJ, Fennell TJ, Stewart C, Lichtenstein L, Meldrim JC, et al. Discovery and characterization of artifactual mutations in deep coverage targeted capture sequencing data due to oxidative DNA damage during sample preparation. Nucleic Acids Res. 2013;41:e67.
45. Kader T, Goode DL, Wong SQ, Connaughton J, Rowley SM, Devereux L, et al. Copy number analysis by low coverage whole genome sequencing using ultra low-input DNA from formalin-fixed paraffin embedded tumor tissue. Genome Med. 2016;8:121.
46. Rieber N, Bohnert R, Ziehm U, Jansen G. Reliability of algorithmic somatic copy number alteration detection from targeted capture data. Bioinformatics. 2017;33:2791–2798.
47. Reis-Filho JS, Lakhani SR. The diagnosis and management of pre-invasive breast disease Genetic alterations in pre-invasive lesions. Breast Cancer Res. 2003;313–9:313–9.
48. Weinstein JN, Collisson EA, Mills GB, Shaw KRM, Ozenberger BA, Ellrott K, et al. The cancer genome atlas pan-cancer analysis project. Nat Genet. 2013;45:1113–20.
49. Chakravarty D, Gao J, Phillips S, Kundra R, Zhang H, Wang J, et al. OncoKB: A Precision Oncology Knowledge Base. JCO Precis Oncol [Internet]. 2017; Available from: http://dx.doi.org/10.1200/PO.17.00011
50. Bose R, Kavuri SM, Searleman AC, Shen W, Shen D, Koboldt DC, et al. Activating HER2 mutations in HER2 gene amplification negative breast cancer. Cancer Discov. 2013;3:224–37.
51. Mujoo K, Choi BK, Huang Z, Zhang N, An Z. Regulation of ERBB3/HER3 signaling in cancer. Oncotarget. 2014;
52. Gerlinger M, Horswell S, Larkin J, Rowan AJ, Salm MP, Varela I, et al. Genomic architecture and evolution of clear cell renal cell carcinomas defined by multiregion sequencing. Nat Genet. 2014;
53. Jones S, Anagnostou V, Lytle K, Parpart-Li S, Nesselbush M, Riley DR, et al. Personalized genomic analyses for cancer mutation discovery and interpretation. Sci Transl Med. 2015;362:911.
54. Martincorena I, Fowler JC, Wabik A, Lawson ARJ, Abascal F, Hall MWJ, et al. Somatic mutant clones colonize the human esophagus with age. Science (80-). 2018;
55. Martincorena I, Roshan A, Gerstung M, Ellis P, Van Loo P, McLaren S, et al. High burden and pervasive positive selection of somatic mutations in normal human skin. Science (80-). 2015;348:880–6.
56. Kalatskaya I, Trinh QM, Spears M, McPherson JD, Bartlett JMS, Stein L. ISOWN: Accurate somatic mutation identification in the absence of normal tissue controls. Genome Med.

2017;9:59.
57. Garofalo A, Sholl L, Reardon B, Taylor-Weiner A, Amin-Mansour A, Miao D, et al. The impact of tumor profiling approaches and genomic data strategies for cancer precision medicine. Genome Med. 2016;9:51.
58. Chen Z, Yuan Y, Chen X, Chen J, Lin S, Li X, et al. Systematic comparison of somatic variant calling performance among different sequencing depth and mutation frequency. Sci Rep. 2020;10:3501.
59. Anzar I, Sverchkova A, Stratford R, Clancy T. NeoMutate: An ensemble machine learning framework for the prediction of somatic mutations in cancer. BMC Med Genomics. 2019;12:63.
60. Yost SE, Smith EN, Schwab RB, Bao L, Jung H, Wang X, et al. Identification of high-confidence somatic mutations in whole genome sequence of formalin-fixed breast cancer specimens. Nucleic Acids Res. 2012;40:e107.
61. Kim H, Lee AJ, Lee J, Chun H, Ju YS, Hong D. FIREVAT: Finding reliable variants without artifacts in human cancer samples using etiologically relevant mutational signatures. Genome Med. 2019;11:81.
62. Hofreiter M. DNA sequences from multiple amplifications reveal artifacts induced by cytosine deamination in ancient DNA. Nucleic Acids Res. 2001;29:4793–9.
63. Tchou J, Grollman AP. Repair of DNA containing the oxidatively-damaged base, 8-oxoguanine. Mutat Res Toxicol. 1993;299:277–87.
64. Chen L, Liu P, Evans TC, Ettwiller LM. DNA damage is a pervasive cause of sequencing errors, directly confounding variant identification. Science (80-). 2017;355:752–6.
65. Kim SY, Jung S-H, Kim MS, Baek I-P, Lee SH, Kim T-M, et al. Genomic differences between pure ductal carcinoma in situ and synchronous ductal carcinoma in situ with invasive breast cancer. Oncotarget. 2015;6:7597–607.
66. Salk JJ, Loubet-Senear K, Maritschnegg E, Valentine CC, Williams LN, Higgins JE, et al. Ultra-Sensitive TP53 Sequencing for Cancer Detection Reveals Progressive Clonal Selection in Normal Tissue over a Century of Human Lifespan. Cell Rep. 2019;28:132–44.
67. Sinha VC, Piwnica-Worms H. Intratumoral Heterogeneity in Ductal Carcinoma In Situ: Chaos and Consequence. J Mammary Gland Biol Neoplasia. 2018;23:191–205.
68. Gerdes MJ, Gökmen-Polar Y, Sui Y, Pang AS, Laplante N, Harris AL, et al. Single-cell heterogeneity in ductal carcinoma in situ of breast. Mod Pathol. 2018;31:406–17.
69. Chin K, De Solorzano CO, Knowles D, Jones A, Chou W, Rodriguez EG, et al. In situ analyses of genome instability in breast cancer. Nat Genet. 2004;36:984–8.
70. Foschini MP, Morandi L, Leonardi E, Flamminio F, Ishikawa Y, Masetti R, et al. Genetic

clonal mapping of in situ and invasive ductal carcinoma indicates the field cancerization phenomenon in the breast. Hum Pathol. 2013;44:1310–9.
71. Martelotto LG, Baslan T, Kendall J, Geyer FC, Burke KA, Spraggon L, et al. Whole-genome single-cell copy number profiling from formalin-fixed paraffin-embedded samples. Nat Med. 2017;23:376–85.
72. Alexandrov LB, Stratton MR. Mutational signatures: The patterns of somatic mutations hidden in cancer genomes. Curr Opin Genet Dev. 2014;24:52–60.
73. Srivastava S, Ghosh S, Kagan J, Mazurchuk R, Boja E, Chuaqui R, et al. The Making of a PreCancer Atlas: Promises, Challenges, and Opportunities. Trends in Cancer. 2019;4:523–36.

Figure Legends

Figure 1. Benchmarking results for sequencing performance. (A) Experimental design for performance evaluation using a test DNA specimen (* Exome and † Cancer panel). **(B-C)** Fraction of targeted bases covered by a minimum of 20 reads (B) and fraction of PCR duplicates (C) observed in whole exome sequencing. **(D-E)** Fraction of targeted bases covered by a minimum of 20 reads (D) and fraction of PCR duplicates (E) observed in cancer panel sequencing.

Figure 2. Benchmarking results for variant calling. **(A-B)** Count of total variants from whole exome sequencing, separated by false positives (red), false negatives (black) and true positives (grey), before (A) and after (B) PML specific filtering. (**C-D)** Exome variant calling precision for various library preparation strategies and amount of input DNA (x-axis) before (C) and after (D) PML specific filtering. (**E-F)** Fraction of the genome involved in a copy number alteration (CNA burden – y axis) for all exome (E) and cancer panel (F) library preparation strategies and DNA input amounts.

Figure 3. Overview of the PML regional sequencing strategy. (A) Overall experimental and analytical workflow of the validation study. **(B)** Images showing the Hematoxylin and Eosin stained sections from the three DCIS patient studied. Dissected PML regions are highlighted in color to the exception of region 3N consisting of multiple areas of normal epithelium outside the selected field of view**.**

Figure 4. Mutational profile and clonal analysis from multi-region DNA sequencing of DCIS patients. (A) Fraction of genome involved in copy number losses (blue) or gains (red) for each sequenced region. **(B)** Chromosome arm copy number status in each sequenced region: lost (blue) or gained (red). (**C)** Cancer gene copy number (log2 ratio – blue red gradient). Genes from the cancer panel with copy number gain (log2(ratio)>0.4) or loss (log2(ratio)<-0.6) in at least one region are displayed. **(D-E)** Bayesian probabilistic variant classification of high confidence somatic variants (represented by their cognate gene – rows) across all dissected regions of same patient (columns). Variants are shown for patient 1 (D) and patient 3 (E). The color gradient indicates the posterior probability of mutation presence in each region. Genes from the Cancer Gene Census are indicated in red font. **(F)** Maximum likelihood tree generated using somatic mutations identified in patient 3's regions.

Figure 1

A

	AT		SS	BE
Specimen	**Frozen**	**FFPE**	**FFPE**	**FFPE**
Library	Standard A-tailing	Standard A-tailing	Single-Strand	Blunt-End
Targeted panel	Exome	Exome / Cancer panel	Exome / Cancer panel	Exome / Cancer panel
Input (ng)	200	200*, 50, 10*, 3	50† , 3	50† , 3

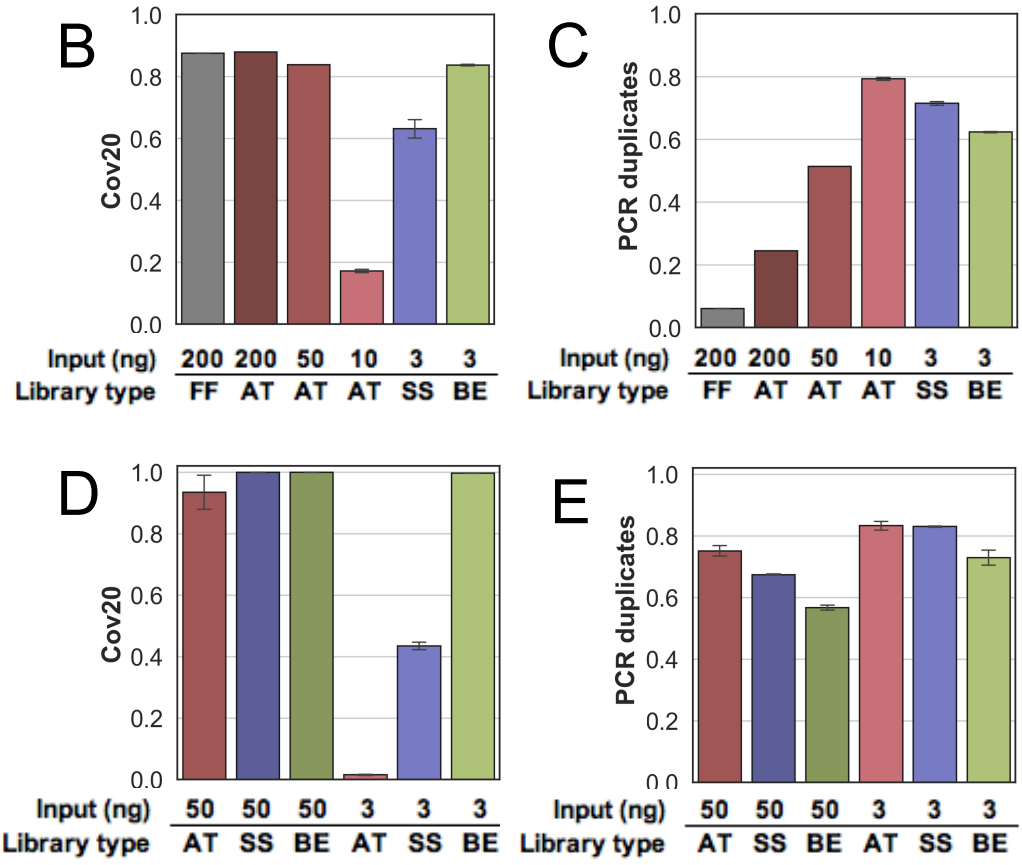

Figure 2

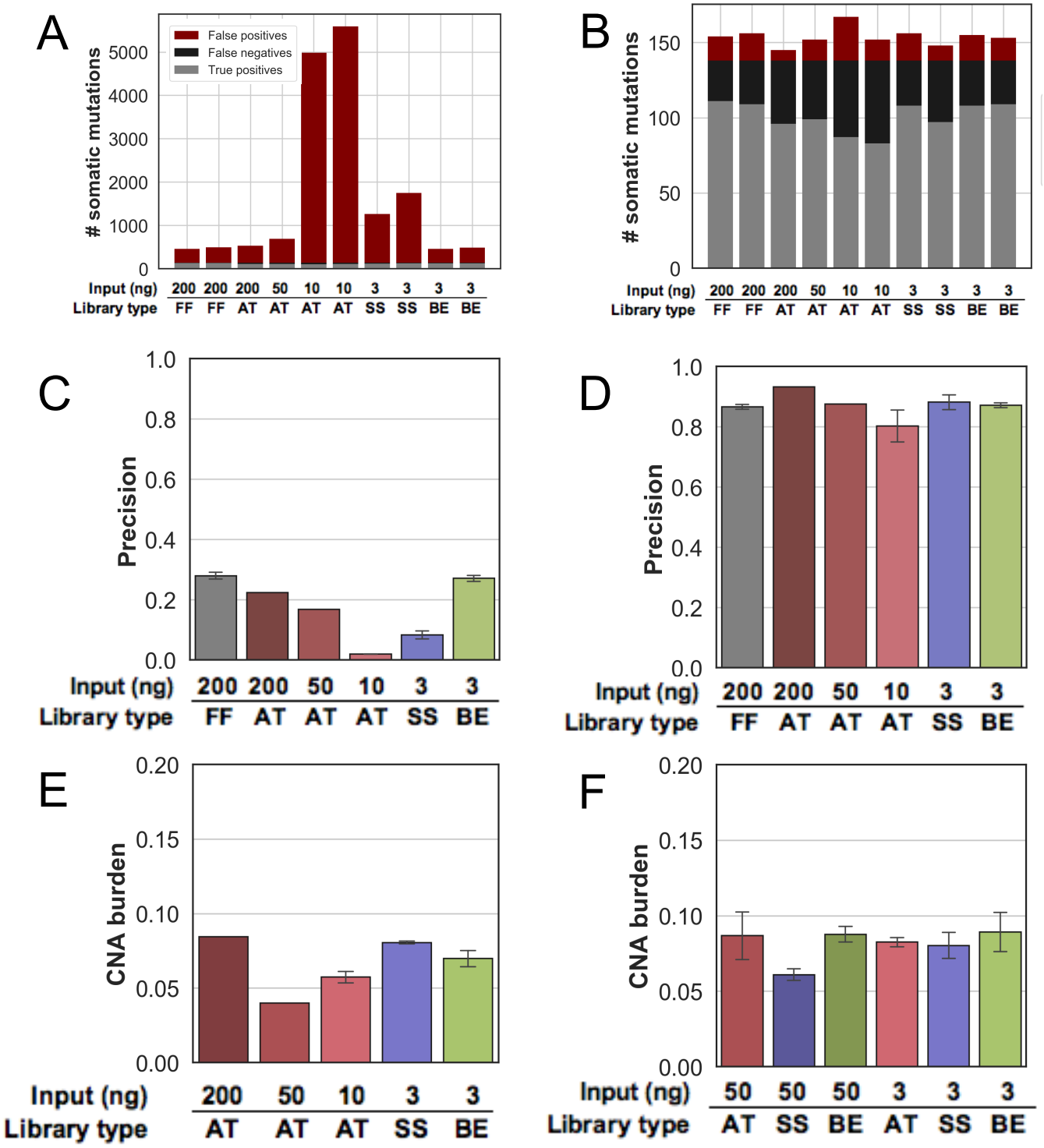
A
False positives
False negatives
True positives
somatic mutations
0
1000
2000
3000
4000
5000
Input (ng) 200 200 200 50 10 10 3 3 3 3
Library type FF FF AT AT AT AT SS SS BE BE
B
somatic mutations
0
50
100
150
Input (ng) 200 200 200 50 10 10 3 3 3 3
Library type FF FF AT AT AT AT SS SS BE BE
C
Precision
0.0
0.2
0.4
0.6
0.8
1.0
Input (ng) 200 200 50 10 3 3
Library type FF AT AT AT SS BE
D
Precision
0.0
0.2
0.4
0.6
0.8
1.0
Input (ng) 200 200 50 10 3 3
Library type FF AT AT AT SS BE
E
CNA burden
0.00
0.05
0.10
0.15
0.20
Input (ng) 200 50 10 3 3
Library type AT AT AT SS BE
F
CNA burden
0.00
0.05
0.10
0.15
0.20
Input (ng) 50 50 50 3 3 3
Library type AT SS BE AT SS BE

Figure 3

A

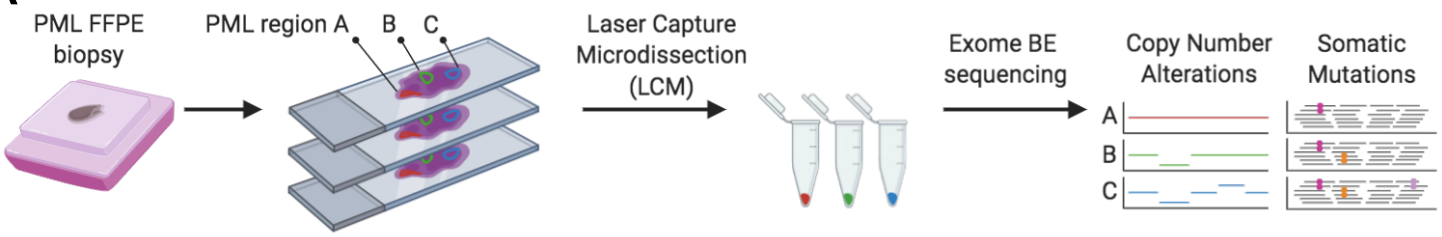
PML FFPE biopsy
PML region A
B
C
Laser Capture Microdissection (LCM)
Exome BE sequencing
Copy Number Alterations
Somatic Mutations
A
B
C

B

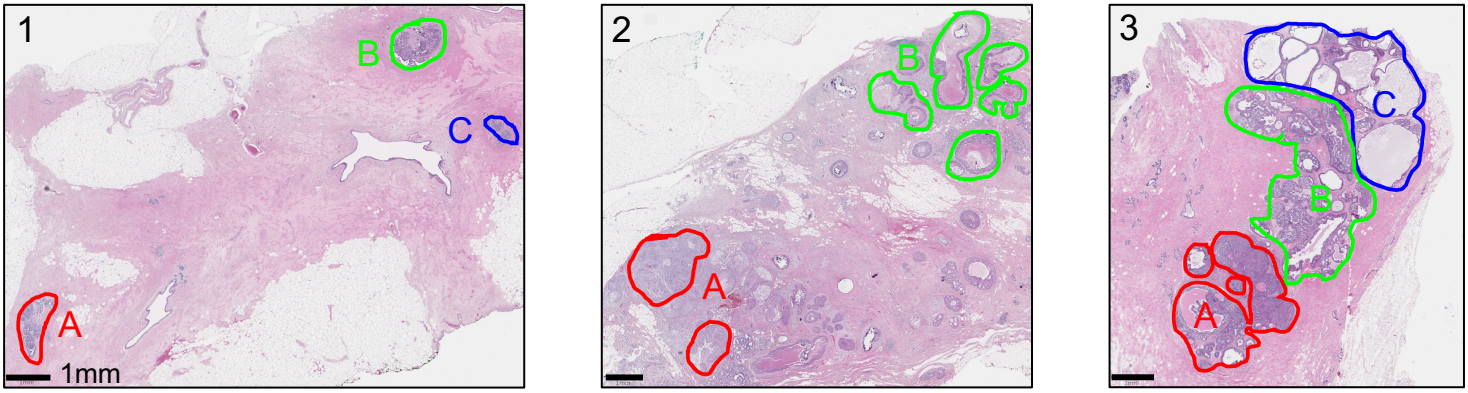
1
B
C
A
1mm
2
B
A
3
C
B
A

Figure 4

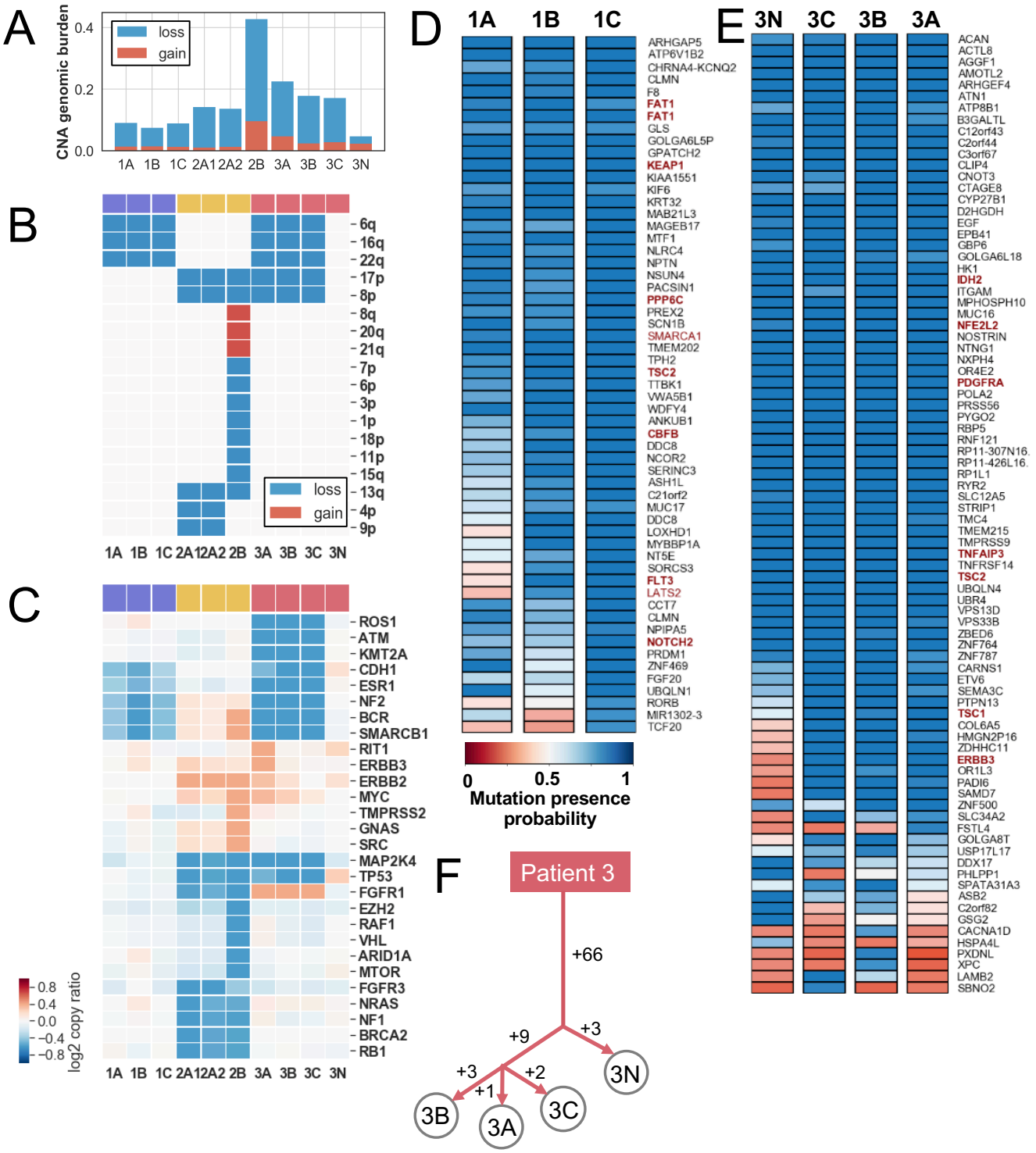
A
CNA genomic burden
0.4
0.2
0.0
loss
gain
1A 1B 1C 2A1 2A2 2B 3A 3B 3C 3N
B
6q
16q
22q
17p
8p
8q
20q
21q
7p
6p
3p
1p
18p
11p
15q
13q
4p
9p
loss
gain
1A 1B 1C 2A1 2A2 2B 3A 3B 3C 3N
C
ROS1
ATM
KMT2A
CDH1
ESR1
NF2
BCR
SMARCB1
RIT1
ERBB3
ERBB2
MYC
TMPRSS2
GNAS
SRC
MAP2K4
TP53
FGFR1
EZH2
RAF1
VHL
ARID1A
MTOR
FGFR3
NRAS
NF1
BRCA2
RB1
0.8
0.4
0.0
−0.4
−0.8
log2 copy ratio
1A 1B 1C 2A1 2A2 2B 3A 3B 3C 3N
D
1A 1B 1C
ARHGAP5
ATP6V1B2
CHRNA4-KCNQ2
CLMN
F8
FAT1
FAT1
GLS
GOLGA6L5P
GPATCH2
KEAP1
KIAA1551
KIF6
KRT32
MAB21L3
MAGEB17
MTF1
NLRC4
NPTN
NSUN4
PACSIN1
PPP6C
PREX2
SCN1B
SMARCA1
TMEM202
TPH2
TSC2
TTBK1
VWA5B1
WDFY4
ANKUB1
CBFB
DDC8
NCOR2
SERINC3
ASH1L
C21orf2
MUC17
DDC8
LOXHD1
MYBBP1A
NT5E
SORCS3
FLT3
LATS2
CCT7
CLMN
NPIPA5
NOTCH2
PRDM1
ZNF469
FGF20
UBQLN1
RORB
MIR1302-3
TCF20
0
0.5
1
Mutation presence probability
E
3N 3C 3B 3A
ACAN
ACTL8
AGGF1
AMOTL2
ARHGEF4
ATN1
ATP8B1
B3GALTL
C12orf43
C2orf44
C3orf67
CLIP4
CNOT3
CTAGE8
CYP27B1
D2HGDH
EGF
EPB41
GBP6
GOLGA6L18
HK1
IDH2
ITGAM
MPHOSPH10
MUC16
NFE2L2
NOSTRIN
NTNG1
NXPH4
OR4E2
PDGFRA
POLA2
PRSS56
PYGO2
RBP5
RNF121
RP11-307N16.
RP11-426L16.
RP1L1
RYR2
SLC12A5
STRIP1
TMC4
TMEM215
TMPRSS9
TNFAIP3
TNFRSF14
TSC2
UBQLN4
UBR4
VPS13D
VPS33B
ZBED6
ZNF764
ZNF787
CARNS1
ETV6
SEMA3C
PTPN13
TSC1
COL6A5
HMGN2P16
ZDHHC11
ERBB3
OR1L3
PADI6
SAMD7
ZNF500
SLC34A2
FSTL4
GOLGA8T
USP17L17
DDX17
PHLPP1
SPATA31A3
ASB2
C2orf82
GSG2
CACNA1D
HSPA4L
PXDNL
XPC
LAMB2
SBNO2
F
Patient 3
+66
+9
+3
+3
+2
+1
3B
3A
3C
3N